

# Thermochemical conversion characteristics of biosolid samples from a wastewater treatment plant in Brisbane, Australia

San Shwe Hla<sup>A</sup>, Nuttaphol Sujarittam<sup>A</sup> and Alexander Ilyushechkin<sup>A,\*</sup> 

**Environmental context.** Biosolids are nutrient-rich organic materials. They can be used as fertiliser and solid amendments in agriculture if treated according to regulatory requirements. If farming applications of biosolids decline due to potential pollution from their heavy metal content, an alternative to traditional methods of biosolid disposal is required. In this context, thermal processing of biosolids is an economically and environmentally suitable option to convert large quantities of biosolids into useful energy.

For full list of author affiliations and declarations see end of paper

**\*Correspondence to:**

Alexander Ilyushechkin  
 CSIRO Energy, PO Box 883, Kenmore  
 4069, Australia  
 Email: [alex.ilyushechkin@csiro.au](mailto:alex.ilyushechkin@csiro.au)

**Handling Editor:**

Ke Sun

**Received:** 7 July 2022

**Accepted:** 5 November 2022

**Published:** 18 January 2023

**Cite this:**

Hla SS *et al.* (2022)  
*Environmental Chemistry*  
 19(6), 385–399. doi:[10.1071/EN22074](https://doi.org/10.1071/EN22074)

© 2022 The Author(s) (or their employer(s)). Published by CSIRO Publishing.

This is an open access article distributed under the Creative Commons Attribution-NonCommercial-NoDerivatives 4.0 International License ([CC BY-NC-ND](https://creativecommons.org/licenses/by-nc-nd/4.0/))

OPEN ACCESS

## ABSTRACT

**Rationale.** Due to more stringent environmental regulations and frequently required long-distance transportation, the traditional disposal of biosolids from wastewater treatment plants in landfills and farms is becoming unsustainable. A potentially economical and environmental option is the thermochemical conversion of biosolids into energy and value-added products. This paper describes the chemical composition and energy content of a representative biosolid sample collected from a major wastewater-treatment plant in Queensland, Australia. **Methodology.** The thermochemical behaviour and compositional changes in biosolids were investigated under a wide range of pyrolysis and gasification conditions using a horizontal tube furnace (HTF), a fixed-bed reactor and a thermogravimetric analyser (TGA). In terms of practical application of by-products, we describe mineral matter transformations in char and ashes during pyrolysis and volatilisation as well as under different gasification conditions. **Results.** HTF experiments revealed that at pyrolysis below 800°C, mainly organic species were released, while losses of inorganic elements (phosphorus, magnesium and zinc) occurred at higher temperatures. *In-situ* gasification behaviour of biosolid chars in the TGA reactor showed that the gasification reaction of biosolid chars occurred rapidly at temperatures above 720°C, regardless of the pyrolysis temperatures at which those chars were produced. Mineral matter transformations began at temperatures above 600°C, and mainly involved the transformation of amorphous phases into crystalline oxide and phosphide forms. Under gasification conditions, all crystalline phases appeared as different phosphates and aluminosilicates. **Discussion.** The methods described here provide different options for the disposal of biosolids from wastewater by adjusting and optimising thermochemical conversion processes.

**Keywords:** ash characteristics, biosolids, gasification, mineral matter, phase transformation, pyrolysis, sewage sludge, thermochemical conversion.

## Introduction

Municipal wastewater contains more than 99% water. After a series of wastewater treatment (WWT) processes, such as screening, sedimentation, aeration, settling and filtration, treated waters are either recycled or discharged depending on their quality and standard classification. During treatment, microorganisms digest the sewage, breaking down the original organic solids. The residues generated in these wastewater treatment processes are called biosolids, also known as sewage sludge. Biosolids are semi-liquid waste containing 75–85% water, with the remaining solids typically made up of organic matter, macronutrients (e.g. nitrogen, phosphorus, potassium, sulfur), micro-nutrients (e.g. copper, zinc, calcium, magnesium, iron) and some inert matter (Darvodelsky 2011). As biosolids are

nutrient-rich, organic materials, they can be used as fertiliser and solid amendments in agriculture if treated according to regulatory requirements (Gonzaga *et al.* 2017). However, farming applications of biosolids are declining due to potential pollution from their heavy metal content (Singh and Agrawal 2008; Gikas 2017). Some European countries have prohibited both using biosolids in agriculture and discarding them in landfill sites to prevent harmful elements entering the human food chain (Fytili and Zabaniotou 2008). In addition, handling biosolids can become a significant challenge for wastewater management industries if distances between WWT plants and permitted agricultural farms are too great for cost-effective transportation (Lundin *et al.* 2004; Donatello and Cheeseman 2013). As an alternative to traditional methods of biosolid disposal, thermal applications are considered to be economically and environmentally suitable options to convert large quantities of biosolids into useful energy at WWT sites (Lundin *et al.* 2004; Cui *et al.* 2006; Calvo *et al.* 2013; Gil-Lalaguna *et al.* 2014).

According to the Australian & New Zealand Biosolids Partnership, 327 000 tonnes of dry biosolids are generated from WWT plants in Australia each year, which is equivalent to 13.6 kg (dry) per person (ANZBP 2017). While European countries are shifting biosolids management methods from land disposal to thermal application, Australia still relies on land disposal: 75% in agriculture, 11% in land rehabilitation, 8% composting and the remaining 6% in stockpiling, landfilling and ocean discharge (ANZBP 2017). Queensland Urban Utilities, a major Australian WWT company, generated 150 000 wet tonnes of biosolids per year from their 28 WWT facilities in Queensland, Australia (Fenwick 2016). They spent approximately AU\$10 million per year transporting biosolids to far-field agricultural land applications, with handling costs alone estimated to be AU\$67 per tonne of wet biosolids. A report released in 2011 estimated the nationwide annual transport cost of biosolids at AU\$60 million (Darvodelsky 2011). Due to high transport costs, increasing awareness of environmental impact and the possibility of more stringent regulations for land disposal methods in the near future, Australia's WWT industries are searching for alternative appropriate solutions to biosolids management.

Extracting energy from biosolids has been regarded as an alternative to disposal, especially as availability and public acceptance of landfilling are decreasing, while the cost of disposal is rising (Nidheesh *et al.* 2021). Tyagi and Lo (2013) and Nidheesh *et al.* (2021) recently reviewed several options for energy recovery from biosolids via thermochemical conversion approaches, including both conventional and emerging methods: incineration and co-combustion, gasification, pyrolysis, supercritical (wet) oxidation and hydrothermal treatment. Of these, supercritical oxidation and hydrothermal treatment are considered to be in the research and development stage, with complexities in reactor design and operation usually associated with elevated capital and maintenance cost (Rulkens and Bien 2004; Tyagi and Lo 2013).

Incinerating biosolids is usually seen by the public as a less favourable option due to concerns about possible harmful emissions. However, modern advanced flue gas-cleaning technologies can effectively reduce and remove all pollutant components and maintain them under regulatory limits (Roy *et al.* 2011). Incineration plants are economically more efficient at the large scale, although this requires higher investment costs. One recommended approach is to mix biosolids with other fuels, such as coal and woody biomass, and use them in existing combustors for heat and power generation (Roy *et al.* 2011; Skoglund *et al.* 2016; Syed-Hassan *et al.* 2017). Cartmell *et al.* (2006) and Roy *et al.* (2011) propose that co-combustion of biosolids with coal and wood pellets would be a cost-effective way to reduce the volume of biosolids while also recovering energy. Interest is growing in gasification, a promising alternative thermal application of biosolids suited to small and medium throughput, which has several advantages over conventional incineration (Saw *et al.* 2012; Tyagi and Lo 2013; Werle 2015). Pyrolysis is another favourable route to convert biosolids into energy and valuable chemicals (Shao *et al.* 2008).

The first stage of the thermochemical conversion process of any solid fuel is devolatilisation. Understanding this phenomenon is therefore important for predicting the behaviour of biosolids during the subsequent stages of combustion and gasification. Several researchers have investigated biosolid devolatilisation under different operating conditions. For instance, Gomez-Barea *et al.* (2010) characterised the devolatilisation behaviour of dried biosolid granulates at 750–900°C using a laboratory fluidised-bed reactor and determined the resulting kinetics parameters. Park *et al.* (2010) studied the product distribution of biosolids under fast pyrolysis conditions at 400–550°C. A similar study by Fairous *et al.* (2010) determined the optimum pyrolysis temperature for bio-oil yield. Fonts *et al.* (2008) examined the effects of operational parameters on pyrolysis product distributions of biosolids to maximise liquid yield. An empirical model developed by Jaramillo-Arango *et al.* (2016) used experimental data tested at 300–800°C to estimate the main pyrolysis products. Finally, Fan *et al.* (2014) used three different biosolid samples to study the yields and composition of gaseous and liquid products using a fixed-bed reactor at 300–700°C.

Despite some lingering technical issues, such as syngas cleaning and tar removal, gasification is usually considered an attractive option for thermochemical conversion of biomass (Tippayawong *et al.* 2013). The technology can be operated at small and medium scales for power generation with higher efficiency and product flexibility, with end products other than heat and power, such as chemicals and liquid fuels, able to be generated (Kirkels and Verbong 2011). The gasification performance of biosolids has been tested in different laboratory-scale gasifiers (Midilli *et al.* 2001; Dogru *et al.* 2002; de Andrés *et al.* 2011a; Arjham *et al.* 2013; Calvo *et al.* 2013; Chun *et al.* 2013; Gil-Lalaguna *et al.* 2014;

Werle and Dudziak 2014), and researchers have carried out fundamental studies of gasification reactions of biosolid chars produced under different pyrolysis conditions (Scott *et al.* 2005; Nowicki *et al.* 2011; Nilsson *et al.* 2012, 2013; Jayaraman and Gökalp 2015; Stylianou *et al.* 2020). Scott *et al.* (2005) compared the reactivity of char produced from dried biosolids with those derived from car tyres, bituminous coals and activated carbon at 800–1050°C, reporting that biosolid-derived char was the most reactive on the basis of both Brunauer–Emmett–Teller surface area and mass. Nilsson *et al.* (2012) used a laboratory fluidised-bed reactor to investigate the reactivity of biosolid char under different partial pressures of CO<sub>2</sub> and H<sub>2</sub>O as reactants. The reaction with H<sub>2</sub>O was approximately three times faster than with CO<sub>2</sub> at 800–900°C, while activation energies for both reactions were similar. The same group (Nilsson *et al.* 2013) extended their reactivity research on biosolid char using a mixture of CO<sub>2</sub>–H<sub>2</sub>O–N<sub>2</sub> and found that char gasification rates for a gas mixture containing both reactants could be approximated as the sum of the individual rates measured separately with CO<sub>2</sub> and H<sub>2</sub>O. In a study of the reactivity of biosolid-derived char using different gaseous agents containing CO<sub>2</sub>, O<sub>2</sub> and H<sub>2</sub>O, Nowicki *et al.* (2011) found that biosolid-derived char reaction with CO<sub>2</sub> and O<sub>2</sub> could be interpreted using a shrinking core model, while expression of the char–steam reaction was more suited to first-order kinetics.

Biosolids cannot be totally eliminated via thermochemical conversion processes, because they contain a large percentage of mineral matter that remain as a form of ash or slag, depending on the thermochemical technologies applied (average value of ~44% in dry basis (db) (Syed-Hassan *et al.* 2017)). These ashes contain harmful substances and should be carefully disposed of in landfill, preventing the possibility of heavy metal leaching from the ashes to the soil–water system (Fytli and Zabaniotou 2008). However, unlike nutrient-poor coal ashes, biosolid ashes contain a large amount of nutrients, especially phosphorus (Donatello and Cheeseman 2013), which can be used in agricultural processes. There are several research and development efforts in the area of treating biosolid ashes to reduce heavy metals and transform the ash into marketable fertiliser products, or products for the construction industry (Donatello and Cheeseman 2013; Cieřlik *et al.* 2015; Herzel *et al.* 2016). Inorganic species in biosolids can also cause serious problems to plant operation due to ash agglomeration, deposition and corrosion on boiler heat-transfer surfaces (Thy *et al.* 2006; Li *et al.* 2013). A better understanding of the release of the inorganic constituents and metals as well as the phase transformation of mineral matter during thermochemical conversion processes is important because biosolids contains harmful compounds and heavy metals. Hwang *et al.* (2007) studied the distribution of heavy metals, such as Cd, Cr, Pb and Zn, in pyrolysis residue (at 500°C) and incineration ash (simulated at 900–1000°C) of biosolids. Saveyn *et al.* (2011) monitored the metal distribution of biosolid chars during the gasification

processes and found that minor elements of the inorganic portion of biosolids are expected to be partially or totally lost due to volatilisation or melting from the biosolids matrix. Similar studies on the transformation and evaporation of heavy metals during pyrolysis and gasification of biosolids have also been conducted (Lu *et al.* 2015; Jin *et al.* 2016; Li *et al.* 2018; Hedayati *et al.* 2021; Hannl *et al.* 2022).

In physical appearance, biosolids appear homogeneous, but their composition, chemical properties, speciation and concentration of heavy metals can vary widely depending on several factors. These include the percentage inclusion of industrial wastewater, the treatment system used at WWT plants, local environmental regulations and seasonal variation (Spanos *et al.* 2016; Tyřta *et al.* 2016; Syed-Hassan *et al.* 2017). Although many overseas researchers have studied behaviour of biosolids under different thermal processes and conditions, work in this area is still limited in Australia, likely due to the lack of industrial practice in converting biosolids to useful energy via thermochemical conversion routes. In this study, we examined the chemical composition and energy content of biosolid samples collected from a major WWT plant in Queensland, Australia. We investigated the compositional changes of biosolids during pyrolysis under a wide range of operating temperatures, gasification characteristics of pyrolysed biosolids using CO<sub>2</sub> and H<sub>2</sub>O as gasifying agents, and mineral matter transformation and volatilisation under different operating temperatures.

## Experimental

### Biosolid sample collection and preparation

Biosolid samples were obtained from Oxley Creek WWT plant, a major sewage treatment facility in Brisbane operated by Queensland Urban Utilities. More than 12 kg of biosolids were collected at the end-point of the entire retreatment processes, once the biosolids had been stabilised and were ready to be transported to farmlands more than 100 km from the plant. Several batches (each batch containing approximately 2 kg of biosolids) were dried in a laboratory oven, with total moisture content measured according to European Standard method ISO 18134-3:2015, which requires the oven temperature to be maintained at 105°C (ISO 2015). To ensure the samples were completely dried, they were initially left in the oven for more than 48 h. After drying, trays of samples were put in a large desiccator to cool to room temperature. They were then weighed immediately to prevent moisture absorption from the atmosphere. The processes of heating, drying, cooling and checking weight were repeated until a total weight change of <0.2% was achieved. The moisture content (wet basis) of the biosolid samples was calculated using the differences in measured sample weight before and after drying. Dry samples were then crushed into particles using a mortar and pestle and sieved to achieve a

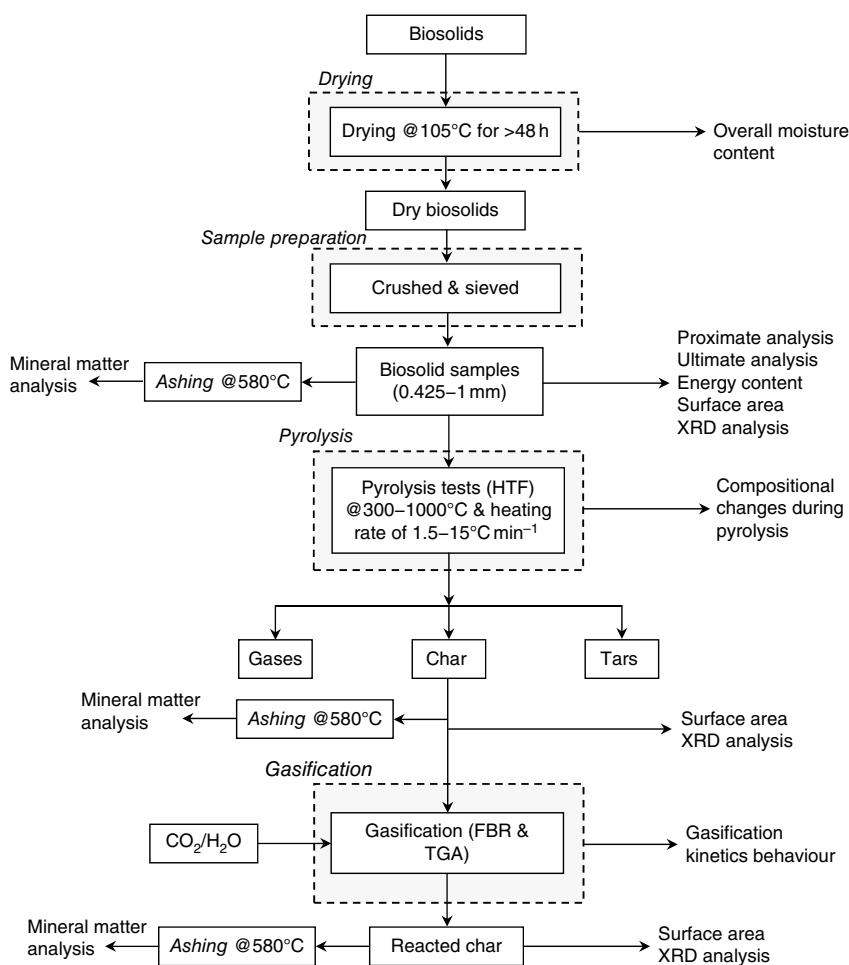


**Fig. 1.** Flow chart for experimental investigation of thermochemical conversion of biosolids. FBR = fixed-bed reactor; HTF = horizontal tube furnace; TGA = thermogravimetric analyser; XRD = X-ray diffraction.

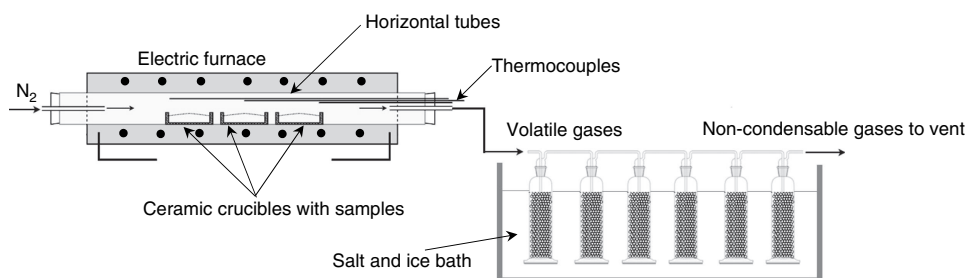


**Fig. 2.** Schematic diagram of experimental rig for pyrolysis tests.

consistent size range between 425  $\mu\text{m}$  and 1 mm. Sized samples were sent to the laboratory for chemical analysis (proximate and ultimate analyses and energy content). In this study, we investigated biosolid properties after pyrolysis and gasification, together with surface area changes in biosolid chars and compositional changes in mineral matter. The sequences and source of samples for the experimental investigations are shown in Fig. 1.

### Experimental rig for pyrolysis test and procedure

Biosolids were pyrolysed using a horizontal tube furnace (HTF) that can be operated at up to 1100°C. Samples

prepared as described above were loaded into two to three laboratory ceramic crucibles located inside a HTF, as shown in Fig. 2. Each tray can be loaded with approximately 10 g of biosolid samples. The reactor was then electrically heated from room temperature to the targeted temperature (300–1000°C) at either a slow heating rate of 1.5°C min<sup>-1</sup> or a median heating rate of 15°C min<sup>-1</sup> (maximum heating rate applicable for HTF), and was maintained at the targeted temperature for 1 h to ensure devolatilisation products were totally removed from the reactor tube. The entire process was conducted under a constant flow (1 L min<sup>-1</sup>) of nitrogen at atmospheric pressure. As shown in Fig. 2, three K-type thermocouples were placed in the left, middle and

right sections of the HTF to ensure consistent temperature distribution. After 1 h at the targeted pyrolysis temperature, the reactor was cooled and the final weight of solid remaining in the crucibles was measured.

Volatile matter released during the experiments was forced out with N<sub>2</sub> flow from the furnace into a series of gas-washing bottles (impingers) filled with a minimum of 150 mL of isopropanol as a sorbent along with laboratory glass beads, as shown in Fig. 2. The impingers were submerged in water cooled by a salt and ice bath. The set up was adapted from the tar protocol defined by the European Committee for Standardization from 2003 to 2005 (Good *et al.* 2005). After each experimental run, the mixture of solvent and condensate from all impingers was rinsed with solvent and mixed in one container. Solvents were then removed under a moderate vacuum of ~10 kPa (abs) at 55°C using a rotary evaporator following the step-by-step procedures described in the tar protocol (Good *et al.* 2005). After evaporation was complete, the total amount of gravimetric tar was calculated using the measured weights of the empty flask and the total weight after solvent evaporation. The total amount of non-condensable gases released during the pyrolysis experiment was calculated using measured solid yield and tar yield.

### Char gasification reactivity tests

A fixed-bed reactor was used for intrinsic reactivity measurement at atmospheric pressure. As shown in Fig. 3, the reactant gases flow through a fixed bed of sample (~1–2 g) supported in a quartz reaction tube by a sintered glass grit. A K-type thermocouple in the bed was used to monitor sample temperatures. After loading the sample as shown in Fig. 3, the reactor was heated by an electric furnace until the

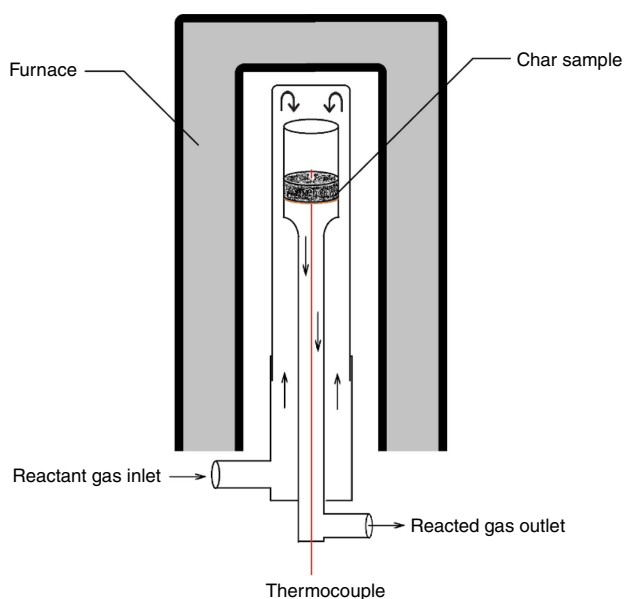


Fig. 3. Schematic diagram of fixed-bed reactor system.

targeted reacting temperature was reached. During the test, operating conditions (reaction temperatures and level of gasification rate targeted) were set to yield about 0.5–0.9% CO to maintain a differential reactor operating mode, where reaction rates are controlled solely by chemical processes without inhibition effects from the products.

For CO<sub>2</sub>-gasification reaction tests, high-purity CO<sub>2</sub> was used to deliver a constant flow of approximately 750 mL min<sup>-1</sup>. For steam-gasification reaction experiments, steam was generated by passing ultra-high purity (99.999%) hydrogen gas over CuO (oxidised Cu wire) heated to 315°C, which oxidised the H<sub>2</sub> to H<sub>2</sub>O as per reaction 1:



One of the advantages of using this method is an ability to control the desired steam flow rate effectively with better accuracy. This method has been successfully and extensively applied in previous research (Roberts and Harris 2000; Hodge 2009). After each experiment, the copper wire was regenerated by heating in air at 315°C for 1–2 h to produce CuO.

The flow rates of reactant gases (N<sub>2</sub>, CO<sub>2</sub> and H<sub>2</sub>O) were controlled by a series of mass flow controllers, each with a maximum flow rate of approximately 1 L<sup>-1</sup> min. Product gas flow was measured with a volumetric gas flow meter, and this, along with the concentration of CO measured using a non-dispersive infrared analyser, was used to calculate the reaction rate. Reaction rates were then calculated from the composition of the feed and product gases and the measured gas flow rates into and out of the reactions, and the mass of the sample before and after reaction. Specific reaction rates in this study were defined as the units of grams of carbon reacting per gram of carbon remaining per second (g g<sup>-1</sup> s<sup>-1</sup>). The procedure and formulas used to estimate reaction rates and kinetic parameters are described in our previous publication (Hla *et al.* 2016).

### Surface area measurement

The surface area of char samples from pyrolysis experiments and gasification tests was determined using adsorption of CO<sub>2</sub> at 273 K and analysis using the Dubinin–Radushkevich equation (Dubinin 1966) and density functional theory model. These measurements are used to calculate the intrinsic reaction rates (defined as the specific rate per unit char surface area) to differentiate the impacts of physical properties of the char samples from those intrinsic to the chemistry of char structure. This approach provides further insights into the gasification behaviour of biosolid chars.

### Thermogravimetric analyser

To understand the *in-situ* transformation under CO<sub>2</sub> gasification conditions, a thermogravimetric analyser (TGA) was used to monitor the changes in mass of different biosolid-

derived chars as a function of time and temperature under atmospheric pressure. Different types of biosolid char samples (produced under pyrolysis conditions at 800, 900 and 1000°C) were loaded in a metal mesh basket (mesh size 100 µm) and suspended in an electrically heated furnace. Their weights were then measured and recorded every 10 s, while a K-type thermocouple located a few millimetres below the sample basket was used to measure and monitor the samples' temperature. Depending on the nature of investigation, a constant flow of CO<sub>2</sub> at 0.3 L min<sup>-1</sup> was supplied either when the reactor's temperature stabilised or during the ramping up to a specific temperature under a heating rate of 1.0°C min<sup>-1</sup>. The raw experimental data, which consisted of time, sample mass and sample temperature, were smoothed and differentiated using software to provide the results at a specific rate (g g<sup>-1</sup> s<sup>-1</sup>).

### Ashing and X-ray diffraction analysis

A large portion of dry biosolids is mineral matter. To investigate the transformation of mineral matter during pyrolysis, all char samples produced at different temperatures were oxidised in a high-temperature muffle furnace to determine the ash content following the European Standard method BS EN 14775 (BSI 2010). X-ray powder diffraction with copper K<sub>α</sub> radiation (λ = 1.5406 Å) was used to identify mineral phases in dry biosolids and biosolid-derived chars under different pyrolysis conditions before and after exposure to gasification tests, and in ash samples produced from dry biosolids and biosolid chars. The X-ray diffraction (XRD) analysis allowed identification of compositional changes in biosolids throughout the thermochemical conversion processes.

## Results and discussion

### Chemical properties of biosolids

The chemical properties of biosolid samples and the standard methods used in this study are listed in Table 1. As described in the experimental section, a large biosolid sample was used to measure the moisture content of biosolid collected from a WWT plant in Brisbane using an international standard method. The results from different batches of drying tests were consistent, with an average value of 74.2% moisture content on a wet basis. This value falls within the typical range of other studies, indicating that raw biosolids contain high levels of water ranging from 71 to 88% (Cartmell et al. 2006; Cui et al. 2006; Roy et al. 2011; Arjharn et al. 2013; Chen et al. 2013; Moon et al. 2015; Gong et al. 2016; Skoglund et al. 2016; Syed-Hassan et al. 2017; Raheem et al. 2018). As explained in Fig. 1, representative biosolid samples were crushed and sieved to a selected size (0.425–1.0 mm) and sent to the laboratory for chemical analysis. The proximate analysis listed in Table 1 show that the biosolids contained 7.9% fixed carbon and

**Table 1.** Chemical analysis of biosolid samples on a dry basis and wet basis.

Analysis	Parameter	Value	Analysis method
Proximate	Total moisture (wt% wb)	74.2	ISO 18134-3:2015 standard
	Volatile matter (wt% db)	52.3	ISO 18123:2015 standard
	Fixed carbon (wt% db)	7.9	ISO 18123:2015 standard
	Ash (wt% db)	39.8	EN 14775:2009 standard
Ultimate	Carbon (wt% db)	31.1	ISO 16948:2015 standard
	Hydrogen (wt% db)	4.7	
	Nitrogen (wt% db)	9.82	
	Oxygen (wt% db)	9.9	
	Sulfur (wt% db)	1.18	ISO 16994:2016 by ICP-OES
Energy content	Gross dry calorific value (MJ kg <sup>-1</sup> )	14.0	EN 14918:2009 standard
	Gross wet calorific value (MJ kg <sup>-1</sup> )	3.43	
	Net dry calorific value (MJ kg <sup>-1</sup> )	13.0	
	Net wet calorific Value (MJ kg <sup>-1</sup> )	3.17	

52.3% volatile matter. These values are similar to those reported by other studies, which listed fixed carbon of 4.4–7.1% and volatile matter content of 46.6–55% (Fonts et al. 2008; Atienza-Martínez et al. 2013; Calvo et al. 2013). The ash content of biosolid samples was 39.8%, significantly higher than other forms of biomass, especially agriculture-derived biomass residue and waste such as rice husk (Quispe et al. 2017; Liu et al. 2020; Zheng et al. 2020) and green waste (Hla and Roberts 2015; Shao et al. 2020), which usually contains a high level of mineral matter. The high ash content of biosolids could cause significant challenges for application in thermochemical conversion systems such as combustion and gasification processes. This is because most facilities are designed for typical woody biomass with low mineral matter that do not require frequent ash removal, and do not cause problems associated with sintering and clinker formation in high-temperature combustion zones (Boström et al. 2012; Arjharn et al. 2013; Skoglund et al. 2016).

From the ultimate analysis described in Table 1, biosolids contained 31% carbon on a dry basis, similar to other studies (Cartmell et al. 2006; Fonts et al. 2008; de Andrés et al. 2011b; Atienza-Martínez et al. 2013; Fuentes-Cano et al. 2013). The carbon content in biosolids is significantly lower than in most biomass and wastes, which contain well above 40% carbon on a dry basis (Hla et al. 2020). The nitrogen content of biosolids was 9.8%, much higher

than that of most biomass and wastes (usually <1% on a dry basis) (Hla *et al.* 2020). The high nitrogen content in biosolids provides fertilising benefits, as it is a major source of plant nutrients (Fytli and Zabaniotou 2008; Gonzaga *et al.* 2017). The higher heating and lower heating values of biosolid samples are also listed in Table 1 on a wet and dry basis. The high moisture content significantly affects the energy content: while heating values were within a medium range on a dry basis, they were very low when moisture content was included on wet basis. Even on a dry basis, the energy content of biosolids was lower than that of most biomass, especially woody material, which usually contains higher than 18 MJ kg<sup>-1</sup> (Hla *et al.* 2020). This low energy content is mainly due to the high level of mineral matter in biosolids.

### Pyrolysis behaviour of biosolids

Yields of total volatile and total solid products were measured under a range of temperature at two different heating rates (Fig. 4). The trend and percentage yields tested under both heating rates were almost identical. The total volatile yield under 15°C min<sup>-1</sup> was slightly higher than that tested under 1.5°C min<sup>-1</sup> for all pyrolysis temperatures; consequently, total solid yield under 15°C min<sup>-1</sup> was slightly less than that tested under 1.5°C min<sup>-1</sup> for all pyrolysis temperatures. One possible explanation is that heating elements in the HTF tended to overshoot the targeted pyrolysis temperatures while testing under the higher heating rate of 15°C min<sup>-1</sup>. These slight variations in product yields are minor – even though the two heating rates varied by an order of magnitude, they both fell well within the slow heating rate category. Due to the design of HTF used in this study, the heating rate could not be increased beyond 15°C min<sup>-1</sup>.

The pyrolysis behaviour of biosolids can be described in three stages: the volatile yield increased significantly between 250 and 400°C, followed by slight increases at 400–800°C, and another significant increase at 800–1000°C (Fig. 4).

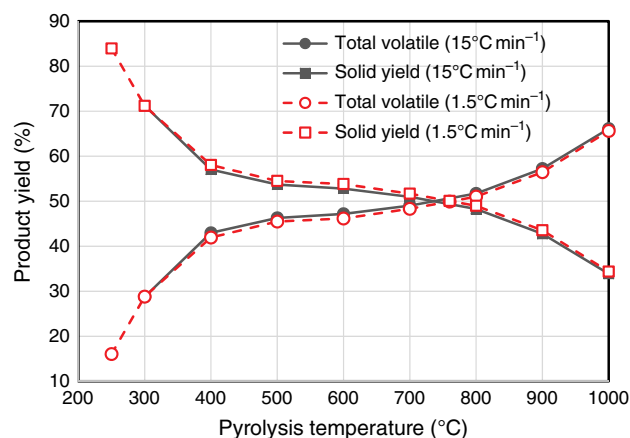


**Fig. 4.** Total volatile and solid yields of biosolids tested under different pyrolysis temperatures.

While the total volatiles released from biosolids during the first two stages of pyrolysis were mainly from organic matter, those released above 800°C originated from both inorganic and organic matter. This is verified by Fig. 5, which shows the variation in ash contents of biosolids measured by ashing the chars produced under different pyrolysis temperatures. These values were calculated using total solid yields measured under each pyrolysis condition using Eqn 2:

$$\begin{aligned} \text{Ash yield of biosolids (wt\% db)} \\ = \text{Ash yield of biosolid char (wt\% db)} \\ \times \text{Total solid yield (wt\% db)} \end{aligned} \quad (2)$$

Fig. 5 shows that ash content measured in biosolid chars produced at 300°C was smaller than that of fresh biosolids. This might be due to release of some inorganic matter under low-temperature pyrolysis conditions. Due to non-oxidising pyrolysis conditions, some mineral matter devolatilised before being converted into oxide phases during ashing, while fresh biosolids under continuous oxidation react with oxygen in the air and form more stable oxides, thus preventing elements from devolatilising. Fig. 5 also reveals that ash yields did not change significantly for biosolid chars produced under pyrolysis temperatures of 300–800°C under both heating rates, but dropped significantly for those biosolid chars produced under pyrolysis temperature above 800°C.

Table 2 lists the chemical composition of ashes from fresh biosolids ashed at 580°C, and from biosolid-derived chars produced at 900°C ashed at 580 or 815°C. The relative content of four oxides (P<sub>2</sub>O<sub>5</sub>, MgO, SO<sub>3</sub> and ZnO) decreased significantly in chars produced at 900°C and was not affected by ashing temperature. The transformation of mineral matter of carbonaceous fuels into gas phases during thermochemical processes has been reported in other studies (Jensen *et al.* 2000; Bläsing and Müller 2013; Gil-Lalaguna *et al.* 2014). The loss of mineral matter under high-temperature pyrolysis

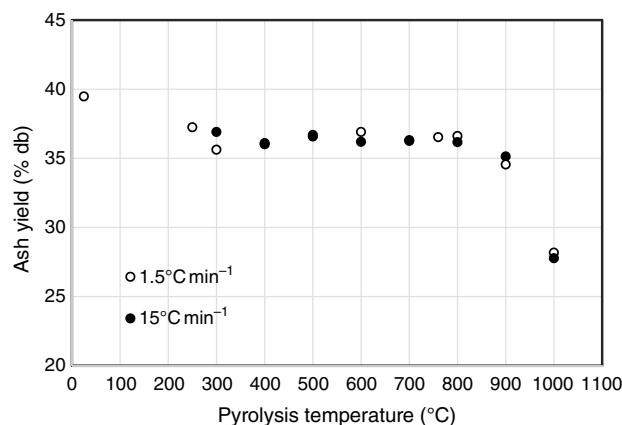


**Fig. 5.** Percentage of ash residue of biosolids measured on a dry basis (db) using chars produced under different pyrolysis temperatures.

**Table 2.** Chemical composition (weight percent of oxides) of ash from fresh biosolids ashed at 580°C (BS01), and biosolid chars produced at a pyrolysis temperature of 900°C and ashed at 815°C (BS02) or 580°C (BS03).

Oxide	BS01	BS02	BS03
SiO <sub>2</sub>	15.6	18.7	18.1
Fe <sub>2</sub> O <sub>3</sub>	12.1	13.8	13.7
Al <sub>2</sub> O <sub>3</sub>	11.1	13.3	13.2
TiO <sub>2</sub>	1.10	1.31	1.31
P <sub>2</sub> O <sub>5</sub>	36.9	31.8	32.4
Mn <sub>3</sub> O <sub>4</sub>	0.12	0.13	0.13
CaO	9.90	11.7	11.6
MgO	8.80	6.00	6.00
Na <sub>2</sub> O	0.65	0.77	0.71
K <sub>2</sub> O	1.94	2.08	2.10
SO <sub>3</sub>	1.32	0.09	0.27
ZnO	0.28	0.06	0.07
BaO	0.11	0.15	0.13
SrO	0.11	0.13	0.13

conditions is associated with volatilisation of some elements at reducing conditions; this will be discussed further in ‘mineral matter transformation’ section.

To check the yields of three major products (gas, tar and char) under different pyrolysis conditions without including the effects of variation of ash content, gas, liquid and solid product yields were plotted on a dry ash-free basis as a function of pyrolysis temperature (Fig. 6). As discussed earlier, the data from two set of experiments tested under two different heating rates were small, so only one set of data are shown, including error bars. Gaseous product yields increased as pyrolysis temperatures rose, but at different rates; yields increased significantly at 300–500°C but only slightly at 500–700°C. Beyond 700°C, gas yields increased sharply, due to a combination of devolatilisation of organic matter and transformation of inorganic matter. Liquid yields initially rose with increasing temperature, remained nearly constant at 500–800°C and decreased slightly above 800°C. This decrease is probably due to the occurrence of secondary reactions of volatiles, such as thermal cracking under high-temperature operating conditions (Fuentes-Cano et al. 2013; Fan et al. 2014; Sattar et al. 2014; Jaramillo-Arango et al. 2016). In contrast to gaseous yield, char yield fell sharply at 300–500°C and then decreased slowly at 500–700°C. Interestingly, char yield decreased significantly beyond 700°C, even to 1000°C, indicating that pyrolysis did not seem to be complete. The remnants of volatile matter in biosolid chars derived from high-temperature pyrolysis has also been reported in other studies (Inguanzo et al. 2001; Shao et al. 2008; Gomez-Barea et al. 2010).

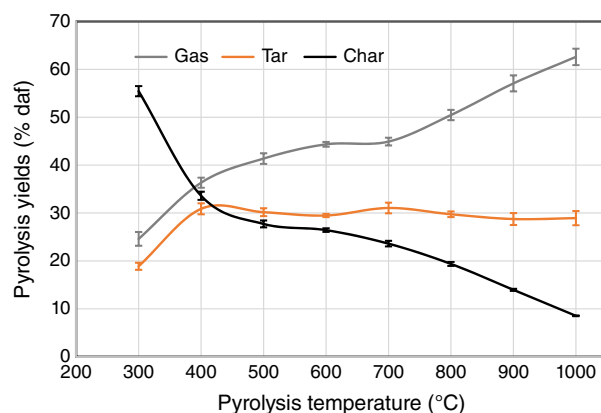


**Fig. 6.** Product yields of biosolids on a dry ash-free (daf) basis as a function of pyrolysis temperature.

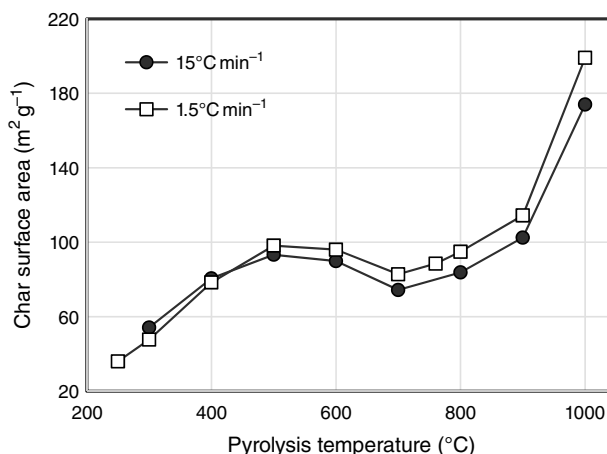


**Fig. 7.** Surface areas of biosolid chars produced under different pyrolysis temperatures.

The total surface areas of biosolid char samples are plotted in Fig. 7 as a function of pyrolysis temperature for both sets of experiments tested under different heating rates. In general, the surface area increased with pyrolysis temperature, with the exception of stabilising between 500 and 800°C and decreasing slightly at 700°C. During the first stage of pyrolysis, the surface area increased almost three-fold from 36 m<sup>2</sup> g<sup>-1</sup> at 250°C to 98 m<sup>2</sup> g<sup>-1</sup> at 500°C. This is attributed to changes in the chemical structure of fresh biosolids, such as an increase in aromaticity, which generates micro and mesopores related to higher surface areas (Agrafioti et al. 2013). The trends seen in Fig. 7 reflect the pyrolysis behaviour of biosolids. When the release of volatile matter slowed between 500 and 800°C, the surface areas were unchanged, except for the slight decrease at 700°C. One possible explanation for the reduction in pore size is that due to the change in phase of some elements in the ash which expanded, the accessible micropore area decreased, and consequently the porosity of the samples decreased (Inguanzo et al. 2001). This explanation corresponds to

the formation of identified crystalline structures above 600°C in the XRD results (see ‘mineral matter transformation’ section). From 800 to 1000°C, as solid yield fell due to the combined effects of transformation of inorganic matter into gaseous phases and devolatilisation of organic matter, the surface areas of the remaining chars doubled. However, this significant increase is insufficient for biosolids to develop surface areas large enough for practical application. The surface areas of biosolid chars in this study are much lower than those associated with commercial activated carbons (often in the order of 1000 m<sup>2</sup> g<sup>-1</sup>) (Xu *et al.* 2017). This is mainly due to the high ash content of biosolids, which hinders the formation of larger surface areas by filling and blocking access to the chars’ micropores (Song and Guo 2012; Agrafioti *et al.* 2013).

### Gasification behaviour of biosolids

The gasification behaviour of biosolid chars produced under three different pyrolysis temperatures (800, 900 and 1000°C) was investigated using a fixed-bed reactor with CO<sub>2</sub> and H<sub>2</sub>O as reactant gases. All experiments were tested at well under 800°C to exclude the effects of devolatilisation during gasification reactions. For each biosolid char sample,

at least three gasification experimental runs were conducted to obtain different carbon conversion levels. Arrhenius plots of the rate data were obtained as samples cooled at the end of each run; the reactivity profiles are shown in Fig. 8. Note this figure only shows the plots that represent char conversion levels between 54 and 63% consumed under the specific gasification reaction tested for those samples. Gasification reaction rates were slower for those samples produced under higher pyrolysis temperatures for both gasification reactions (C + CO<sub>2</sub>, C + H<sub>2</sub>O) investigated. This is probably due to changes in crystalline structure of the chars produced at higher pyrolysis temperatures, which provides a catalytic effect favouring the metal oxidation reactions competing with char gasification reactions. As we discuss in the next section, some crystalline structures formed for those chars produced at pyrolysis of 760°C and more crystalline phases formed with increasing pyrolysis temperatures above 760°C. The gasification reactant gases may therefore tend to react with these crystalline structures, and not just with the carbon from chars. Consequently, this phenomenon will slow the gasification reactions, especially for those chars produced at high temperatures (900 and 1000°C).

The Arrhenius plots of the rate data presented in Fig. 8 were taken from the experimental runs for the char–CO<sub>2</sub> reaction with 100% CO<sub>2</sub> or 30% H<sub>2</sub>O as reactants. We did not determine the reaction order of H<sub>2</sub>O, as it was outside the scope of this study. Thus, these two sets of experimental results cannot be directly compared. Nevertheless, even with only 30% H<sub>2</sub>O, it was clear that like other biomasses, biosolid chars are more reactive with H<sub>2</sub>O than with CO<sub>2</sub> (Nowicki *et al.* 2011). Table 3 lists the kinetic parameters measured for six sets of gasification experiments. The activation energies were in a narrow range of 184–202 kJ mol<sup>-1</sup> for the char–H<sub>2</sub>O reaction and 218–227 kJ mol<sup>-1</sup> for the char–CO<sub>2</sub> reaction.

The trend of char surface areas changes during the two gasification reactions is shown in Fig. 9. Char surface area was measured after each gasification experiment using a fixed-bed reactor, which provided changes in the profile of char structure at different levels of carbon conversion. During both gasification reactions, char surface area did

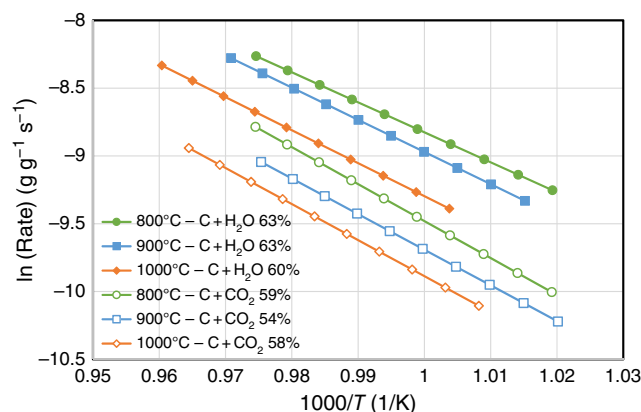


**Fig. 8.** Arrhenius plots of specific reaction rate for chars from biosolids generated under three pyrolysis temperatures.

**Table 3.** Kinetic parameters measured for char–CO<sub>2</sub> and char–H<sub>2</sub>O gasification reactions for biosolid chars produced under three different pyrolysis temperatures.

Pyrolysis temperature (°C)	Reaction	Carbon conversion after gasification reaction (%)	Pre-exponential factor (g g <sup>-1</sup> s <sup>-1</sup> )	Activation energy (kJ mol <sup>-1</sup> )
800	C + CO <sub>2</sub> = 2CO	59.2	5.3 × 10 <sup>7</sup>	226.7
900	C + CO <sub>2</sub> = 2CO	54.0	1.6 × 10 <sup>7</sup>	218.5
1000	C + CO <sub>2</sub> = 2CO	58.1	1.8 × 10 <sup>7</sup>	221.1
800	C + H <sub>2</sub> O = CO + H <sub>2</sub>	62.6	6.0 × 10 <sup>5</sup>	184.0
900	C + H <sub>2</sub> O = CO + H <sub>2</sub>	62.9	2.6 × 10 <sup>6</sup>	197.4
1000	C + H <sub>2</sub> O = CO + H <sub>2</sub>	60.3	3.4 × 10 <sup>6</sup>	202.4

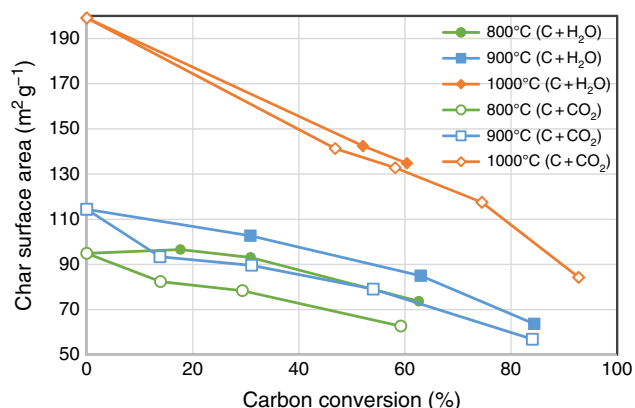


**Fig. 9.** Changes in surface area of biosolid chars during gasification reactions.

not significantly increase; instead, it decreased monotonically as conversion increased for all cases. This is consistent with the expectation discussed in the previous section that these chars have low porosity, particularly lacking micropores, due to the high mineral matter of biosolids blocking the formation of porous structures. Decreases of char surface area during the char–H<sub>2</sub>O reaction were more gradual than in the char–CO<sub>2</sub> reaction, but these differences were minor.

Biosolid char samples were also tested in two different sets of TGA runs using CO<sub>2</sub> as a reactant to understand *in-situ* transformation under gasification conditions. The first set tested the gasification behaviour of samples produced under pyrolysis conditions at 800, 900 and 1000°C under a constant, stable gasification temperature of 750°C. The second set investigated gasification behaviour of samples while ramping the temperature up to a specific targeted value under a constant heating rate of 1.0°C min<sup>-1</sup>. During this set, the maximum gasification temperature was maintained well below the pyrolysis temperature at which respective char sample was produced to avoid devolatilisation effects during gasification. Fig. 10 shows the changes in mass as a function of temperature under a constant gasification temperature of 750°C. At the beginning of the TGA runs, the mass of the samples increased before falling due to the char–CO<sub>2</sub> gasification reaction. The higher the pyrolysis temperature at which the char sample was generated, the more apparent the initial increase at the beginning of the run. This phenomenon is uncommon in TGA tests for chars with low ash content, but can be explained by XRD analysis of the samples before and after gasification reactions. This showed that char generated at higher pyrolysis temperatures had a higher percentage of ashes and favoured the metal oxidising reaction, which increased the mass before the gasification reaction could occur. A similar finding was reported in a study of the kinetics of gasification for char derived from sewage sludge (Nowicki *et al.* 2011). Fig. 10 shows that weight loss percentage at the end of the TGA runs was smaller for those chars produced under a higher

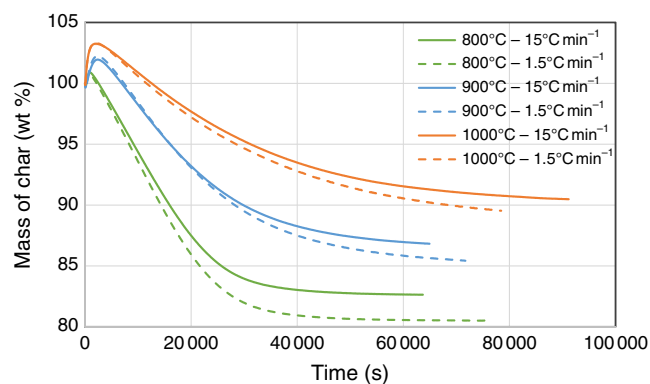


**Fig. 10.** Change in mass percentage of biosolid chars produced under different pyrolysis conditions vs time during CO<sub>2</sub> gasification reaction at constant temperature of 750°C, tested using a thermogravimetric analyser.

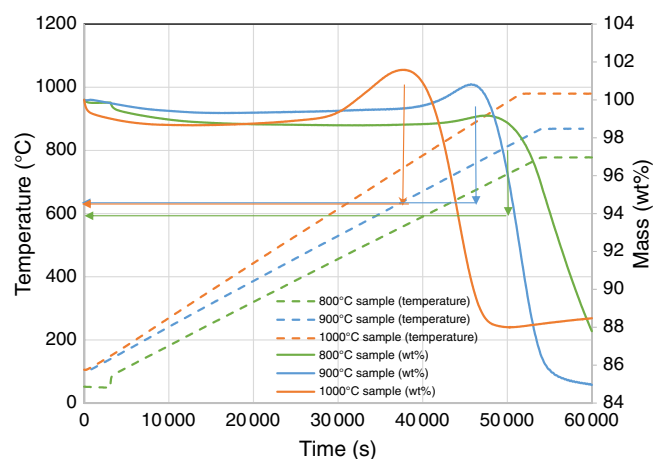


**Fig. 11.** Change in mass percentage of biosolid chars produced under different pyrolysis conditions vs time during CO<sub>2</sub> gasification reaction under increasing temperatures, tested using a thermogravimetric analyser.

heating rate (15°C min<sup>-1</sup>) than those produced under a lower heating rate (1.5°C min<sup>-1</sup>). This phenomenon could be explained by the marginally smaller total solid yield produced under the higher heating rate, due to a possible slight overshoot of the targeted temperatures during pyrolysis experiments (see the previous section).

Fig. 11 shows the *in-situ* gasification behaviour of biosolid chars at increasing temperatures in the TGA reactor. The biosolid chars began to rapidly undergo gasification at temperatures above 720°C, regardless of the pyrolysis temperatures at which those chars were produced. As shown by the XRD analysis as discussed in the next section, the metal oxidation reaction started at a lower temperature of around 600°C, meaning it has a lower activation energy, and is thus expected to occur faster than the gasification reaction. This might be why the metal oxidation reaction dominated the beginning of the gasification experiment, as

shown in Fig. 10, thereby increasing the mass of char samples. After the metals in the samples had been oxidised, the overall reaction would lean towards gasification, explaining why the total mass started decreasing gradually after a short period.

### Mineral matter transformation under thermochemical conversion of biosolids

In original dried biosolids, similar to other types of biomass, most inorganic matter consists of amorphous inorganic phases and poorly crystallised mineraloids from various groups and classes (Vassilev *et al.* 2012). While volatiles are released during biosolid pyrolysis reactions, several crystalline phases are formed in biosolid chars as a result of decomposition of salts and hydrocarbons, particularly at high temperatures. The XRD spectra of chars processed at different pyrolysis temperatures are shown in Fig. 12.

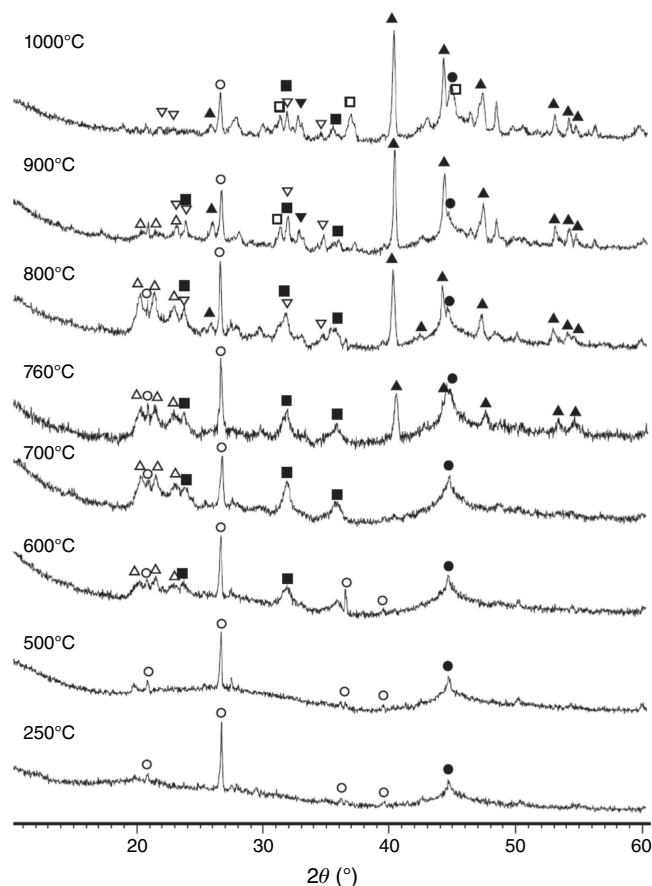
Mineral matters in chars at low temperatures were mainly present in an amorphous form. At  $T < 600^\circ\text{C}$ , only  $\text{SiO}_2$  is present in crystalline phase as quartz. At pyrolysis temperatures of  $600^\circ\text{C}$  and above,  $\text{AlPO}_4$  and  $\text{Al}_2\text{CaSi}_2\text{O}_8$

began to form.  $\text{Fe}_2\text{P}$  started to form above  $700^\circ\text{C}$  and became a dominant phase at higher temperatures. Some phosphorus appeared in oxide form as stanfieldite at  $900^\circ\text{C}$  and above. At these temperatures spinel and possibly hematite were formed, while  $\text{AlPO}_4$  disappeared in char prepared at  $1000^\circ\text{C}$ .

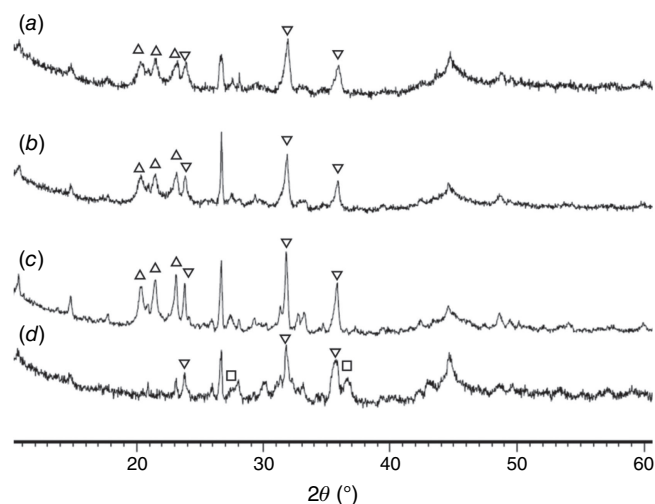
Fig. 13 shows the XRD patterns for pyrolysis chars prepared at  $760$ – $1000^\circ\text{C}$  and then processed in  $\text{CO}_2$  (fixed-bed reactor). As indicated,  $\text{Fe}_2\text{P}$  peaks diminished during gasification, especially in chars prepared at  $760$  and  $800^\circ\text{C}$ , while stanfieldite  $\text{Ca}_4\text{Mg}_5(\text{PO}_4)_6$  and  $\text{AlPO}_4$  phases increased in processed chars with temperature. As  $\text{Fe}_2\text{P}$  content was highest in chars prepared at  $900^\circ\text{C}$ , the highest  $\text{Ca}_4(\text{Mg}_5(\text{PO}_4)_6)$  and  $\text{AlPO}_4$  peaks were observed in chars gasified in  $\text{CO}_2$  at  $900^\circ\text{C}$  accordingly. Crystallinity in gasified chars processed at pyrolysis temperature of  $1000^\circ\text{C}$  was lower than in gasified chars processed at lower pyrolysis temperatures. The  $\text{AlPO}_4$  phase disappeared in gasified chars processed at  $1000^\circ\text{C}$ .

Fig. 14 shows the phase compositions of pyrolysis chars prepared at  $760$ – $1000^\circ\text{C}$  and processed in  $\text{H}_2\text{O}$  (FBR reactor).  $\text{Fe}_2\text{P}$  peaks were not detected in any of these chars, and the crystallinity of oxide phases did not change at  $750$ – $900^\circ\text{C}$ . Overall, very similar crystalline structures were observed in chars processed with  $\text{CO}_2$  and  $\text{H}_2\text{O}$  as reactant gases. Chars prepared at  $760$  and  $800^\circ\text{C}$  and gasified with  $\text{H}_2\text{O}$  had higher crystallinity in formed oxide phases (Fig. 14a, b) than in chars processed in  $\text{CO}_2$  (Fig. 13a, b), indicating more reactive gasification conditions in the presence of  $\text{H}_2\text{O}$ .

During pyrolysis, gaseous oxygen is unavailable and there is insufficient oxygen from volatile species to form all minerals in crystalline oxide form. Only some Si, Al or Ca starts to form calcium-alumino silicate, alumino or alumino-magnesium phosphate fine particles (as demonstrated by



**Fig. 12.** X-ray diffraction patterns of chars processed at different temperatures. Legend:  $\circ = \text{SiO}_2$ ,  $\blacktriangle = \text{Fe}_2\text{P}$ ,  $\triangle = \text{AlPO}_4$ ,  $\blacksquare = \text{Al}_2\text{CaSi}_2\text{O}_8$ ,  $\nabla = \text{stanfieldite}$ ,  $\square = \text{spinel}$ ,  $\blacksquare = \text{Ca}_4\text{Mg}_5(\text{PO}_4)_6$ ,  $\blacktriangledown = \text{Mg}_x\text{Fe}_{1-x}\text{Al}_2\text{O}_4$ ,  $\bullet = \text{carbon}$ .



**Fig. 13.** X-ray diffraction patterns of samples processed in fixed-bed reactor with  $\text{CO}_2$ : chars prepared at  $760^\circ\text{C}$  (a),  $800^\circ\text{C}$  (b),  $900^\circ\text{C}$  (c) and  $1000^\circ\text{C}$  (d). Legend:  $\nabla = \text{stanfieldite}$ ,  $\blacktriangledown = \text{Ca}_4\text{Mg}_5(\text{PO}_4)_6$ ,  $\triangle = \text{aluminium phosphate, AlPO}_4$ ,  $\square = \text{spinel}$ ,  $\bullet = \text{Mg}_x\text{Fe}_{1-x}\text{Al}_2\text{O}_4$ .

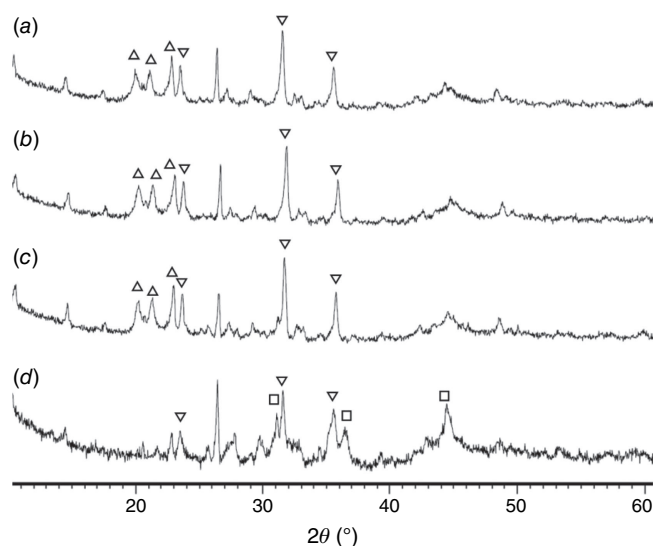


**Fig. 14.** X-ray diffraction patterns of samples processed in fixed-bed reactor with  $\text{H}_2\text{O}$ : chars prepared at  $760^\circ\text{C}$  (a),  $800^\circ\text{C}$  (b),  $900^\circ\text{C}$  (c) and  $1000^\circ\text{C}$  (d). Legend:  $\nabla$  = stanfieldite,  $\text{Ca}_4\text{Mg}_5(\text{PO}_4)_6$ ,  $\triangle$  = aluminium phosphate,  $\text{AlPO}_4$ ,  $\square$  = spinel,  $\text{Mg,Fe}_{1-x}\text{Al}_2\text{O}_4$ .

the broad XRD peaks in Fig. 12). Only a small part of Fe forms spinel and hematite above  $900^\circ\text{C}$ , while most Fe and P are not oxidised and instead form iron phosphide,  $\text{Fe}_2\text{P}$ . The appearance of  $\text{Fe}_2\text{P}$  in chars obtained from pyrolysis of sewage sludge at  $950^\circ\text{C}$  has been reported (Seredych and Badosz 2007), and the degree of crystallisation in processed chars increased with temperature and pyrolysis time. This indicates that the kinetics of crystallised mineral formation is important in terms of the appearance of different phases of solid products from pyrolysis and gasification processes. Further investigation is necessary to explore this phenomenon in more detail.

When gasification reactions begin, sufficient oxygen is available to oxidise phosphide and transfer minerals to  $\text{Ca}_4\text{Mg}_5(\text{PO}_4)_6$  and  $\text{AlPO}_4$  phases by reacting with Ca and Mg from amorphous phases and possibly from existing crystalline phases. In gasification reactions, the crystallinity of  $\text{Ca}_4\text{Mg}_5(\text{PO}_4)_6$  and  $\text{AlPO}_4$  phases increases slightly compared with other crystalline phases. This might indicate that more cations are available from the amorphous phase while chars are processed under gasification conditions. The crystallinity of phases in chars processed at  $1000^\circ\text{C}$  are lower and could be associated with losses of P at this temperature.

As mentioned earlier, processing chars at temperatures above  $900^\circ\text{C}$  results in some losses of inorganic elements, particularly, P, Zn and Mg, which could bond with volatile phases. However, P and Zn could be potentially recaptured from (migrated to) ashes produced under real gasification conditions depending on the type of solid by-products and the sewage sludge used (Werle and Dudziak 2014).

For practical application of thermochemically processed biosolids and their by-products, subsequent studies will aim

to understand the specific conditions for the formation of particular inorganic species (e.g. those containing phosphorus), and to identify how their key characteristics are affected by different processing conditions.

## Conclusions

In this study, biosolid samples collected from a major WWT plant in Queensland, Australia were thermochemically treated and subsequently characterised under a wide range of operating conditions. The unique properties of biosolids include significantly high moisture content and mineral matter compared with other biomasses and wastes. Biosolid carbon content is lower than most other biomass and wastes, although their nitrogen content (9.8%) is much higher, making them potentially suitable for use in fertilisers. The energy content of biosolids is low, mainly due to their high level of mineral matter, which also affects gasification reactions in biosolid chars. Gas yield during pyrolysis increased significantly from  $300\text{--}500$  to  $800\text{--}1000^\circ\text{C}$ , while char yield decreased accordingly in the same temperature ranges. Pyrolysis temperature also affects the organic and inorganic matter released from biosolids. Below  $800^\circ\text{C}$ , mainly organic species were released, while at higher temperatures losses of phosphorus, magnesium and zinc occurred. Mineral matter in chars pyrolysed at temperatures below  $600^\circ\text{C}$  appears in an amorphous form, but at higher temperatures it is transformed into crystalline phases as oxides and phosphides. Like other carbonaceous solid fuels, biosolid chars are more reactive with  $\text{H}_2\text{O}$  than  $\text{CO}_2$ . Under gasification conditions, all crystalline phases in chars appear in oxide forms and their crystallinity is higher in the presence of  $\text{H}_2\text{O}$ , indicating more oxidised conditions. Phosphorus appeared in different forms in biosolid chars under pyrolysis and gasification conditions. The findings from this study clearly show the significance of operating parameters and conditions on the properties of the produced biosolid chars and ashes. Our extensive analyses demonstrate the possibility that by modifying and optimising thermochemical conversion processes, the properties of by-products from biosolids could be adjusted for potential practical application. Future studies should investigate the kinetics of mineral crystallisation and the possible catalytic effect of some minerals in biosolids on gas-phase reactions.

## References

- Agrafioti E, Bouras G, Kalderis D, Diamadopoulos E (2013) Biochar production by sewage sludge pyrolysis. *Journal of Analytical and Applied Pyrolysis* **101**, 72–78. doi:10.1016/j.jaap.2013.02.010
- ANZBP (2017) Australian Biosolids Statistics: Biosolids production in Australia - 2017. Available at <https://www.biosolids.com.au/guidelines/australian-biosolids-statistics/> [verified on 9 December 2022]
- Arjharh W, Hinsui T, Liplap P, Raghavan GSV (2013) Evaluation of an Energy Production System from Sewage Sludge Using a Pilot-Scale

- Downdraft Gasifier. *Energy & Fuels* **27**(1), 229–236. doi:10.1021/ef3012728
- Atienza-Martínez M, Fonts I, Ábrego J, Ceamanos J, Gea G (2013) Sewage sludge torrefaction in a fluidized bed reactor. *Chemical Engineering Journal* **222**(Supplement C), 534–545. doi:10.1016/j.cej.2013.02.075
- Bläsing M, Müller M (2013) Release of alkali metal, sulphur, and chlorine species from high temperature gasification of high- and low-rank coals. *Fuel Processing Technology* **106**, 289–294. doi:10.1016/j.fuproc.2012.08.010
- Boström D, Skoglund N, Grimm A, Boman C, Öhman M, Broström M, Backman R (2012) Ash Transformation Chemistry during Combustion of Biomass. *Energy & Fuels* **26**(1), 85–93. doi:10.1021/ef201205b
- BSI (2010) BS EN 14775:2009 – Solid biofuels. Determination of ash content. The British Standards Institution. <https://doi.org/10.3403/30198062>
- Calvo LF, García AI, Otero M (2013) An Experimental Investigation of Sewage Sludge Gasification in a Fluidized Bed Reactor. *The Scientific World Journal* **2013**, 479403. doi:10.1155/2013/479403
- Cartmell E, Gostelow P, Riddell-Black D, Simms N, Oakey J, Morris J, Jeffrey P, Howsam P, Pollard SJ (2006) Biosolids—A Fuel or a Waste? An Integrated Appraisal of Five Co-combustion Scenarios with Policy Analysis. *Environmental Science & Technology* **40**(3), 649–658. doi:10.1021/es052181g
- Chen Y, Guo L, Jin H, Yin J, Lu Y, Zhang X (2013) An experimental investigation of sewage sludge gasification in near and supercritical water using a batch reactor. *International Journal of Hydrogen Energy* **38**(29), 12912–12920. doi:10.1016/j.ijhydene.2013.05.076
- Chun YN, Ji DW, Yoshikawa K (2013) Pyrolysis and gasification characterization of sewage sludge for high quality gas and char production. *Journal of Mechanical Science and Technology* **27**(1), 263–272. doi:10.1007/s12206-012-1202-0
- Cieslik BM, Namieśnik J, Konieczka P (2015) Review of sewage sludge management: standards, regulations and analytical methods. *Journal of Cleaner Production* **90**, 1–15. doi:10.1016/j.jclepro.2014.11.031
- Cui H, Ninomiya Y, Masui M, Mizukoshi H, Sakano T, Kanaoka C (2006) Fundamental Behaviors in Combustion of Raw Sewage Sludge. *Energy & Fuels* **20**(1), 77–83. doi:10.1021/ef050188d
- Darvodelsky P (2011) Biosolids snapshot. The Department of Sustainability, Environment, Water, Population and Communities. Australia. <https://www.agriculture.gov.au/sites/default/files/documents/biosolids-snapshot.pdf> [verified on 9 December 2022]
- de Andrés JM, Narros A, Rodríguez ME (2011a) Air-steam gasification of sewage sludge in a bubbling bed reactor: Effect of alumina as a primary catalyst. *Fuel Processing Technology* **92**(3), 433–440. doi:10.1016/j.fuproc.2010.10.006
- de Andrés JM, Narros A, Rodríguez ME (2011b) Behaviour of dolomite, olivine and alumina as primary catalysts in air-steam gasification of sewage sludge. *Fuel* **90**(2), 521–527. doi:10.1016/j.fuel.2010.09.043
- Dogru M, Midilli A, Howarth CR (2002) Gasification of sewage sludge using a throated downdraft gasifier and uncertainty analysis. *Fuel Processing Technology* **75**(1), 55–82. doi:10.1016/S0378-3820(01)00234-X
- Donatello S, Cheeseman CR (2013) Recycling and recovery routes for incinerated sewage sludge ash (ISSA): a review. *Waste Management* **33**(11), 2328–2340. doi:10.1016/j.wasman.2013.05.024
- Dubinín MM (1966) Porous structure and adsorption properties of active carbons. In ‘Chemistry and Physics of Carbon. Vol. 2’. (Ed. PJ Walker Jr) pp. 51–120. (Marcel Dekker: New York)
- Fairous S, Rusnah S, Maryam H (2010) Potential source of bio-fuel from pyrolysis of treated sewage sludge. In ‘2010 International Conference on Science and Social Research (CSSR 2010)’, 5–7 December 2010, Kuala Lumpur, Malaysia. pp. 1272–1277 (IEEE) doi:10.1109/CSSR.2010.5773732
- Fan H, Zhou H, Wang J (2014) Pyrolysis of municipal sewage sludges in a slowly heating and gas sweeping fixed-bed reactor. *Energy Conversion and Management* **88**(Supplement C), 1151–1158. doi:10.1016/j.enconman.2014.05.043
- Fenwick G (2016) Achieving the biosolids strategy at Sandgate Sewage Treatment Plant. In ‘79th Annual WIOA Victorian Water Industry Operations Conference and Exhibition’. 31 August–1 September 2016, Bendigo, VIC, Australia. (Water Industry Operators Association of Australia (WIOA)). Available at [http://www.wioa.org.au/conference\\_papers/2016\\_vic/documents/Gary\\_Fenwick.pdf](http://www.wioa.org.au/conference_papers/2016_vic/documents/Gary_Fenwick.pdf)
- Fonts I, Juan A, Gea G, Murillo MB, Sánchez JL (2008) Sewage Sludge Pyrolysis in Fluidized Bed, 1: Influence of Operational Conditions on the Product Distribution. *Industrial & Engineering Chemistry Research* **47**(15), 5376–5385. doi:10.1021/ie7017788
- Fuentes-Cano D, Gómez-Barea A, Nilsson S, Ollero P (2013) The influence of temperature and steam on the yields of tar and light hydrocarbon compounds during devolatilization of dried sewage sludge in a fluidized bed. *Fuel* **108**(Supplement C), 341–350. doi:10.1016/j.fuel.2013.01.022
- Fyttili D, Zabaniotou A (2008) Utilization of sewage sludge in EU application of old and new methods—A review. *Renewable and Sustainable Energy Reviews* **12**(1), 116–140. doi:10.1016/j.rser.2006.05.014
- Gikas P (2017) Ultra high temperature gasification of municipal wastewater primary biosolids in a rotary kiln reactor for the production of synthesis gas. *Journal of Environmental Management* **203**(Part 2), 688–694. doi:10.1016/j.jenvman.2016.02.043
- Gil-Lalaguna N, Sánchez JL, Murillo MB, Rodríguez E, Gea G (2014) Air-steam gasification of sewage sludge in a fluidized bed. Influence of some operating conditions. *Chemical Engineering Journal* **248**(Supplement C), 373–382. doi:10.1016/j.cej.2014.03.055
- Gomez-Barea A, Nilsson S, Vidal Barrero F, Campoy M (2010) Devolatilization of wood and wastes in fluidized bed. *Fuel Processing Technology* **91**(11), 1624–1633. doi:10.1016/j.fuproc.2010.06.011
- Gong M, Zhu W, Fan Y, Zhang H, Su Y (2016) Influence of the reactant carbon-hydrogen-oxygen composition on the key products of the direct gasification of dewatered sewage sludge in supercritical water. *Bioresource Technology* **208**(Supplement C), 81–86. doi:10.1016/j.biortech.2016.02.070
- Gonzaga MIS, Mackowiak CL, Comerford NB, Moline EFdV, Shirley JP, Guimaraes DV (2017) Pyrolysis methods impact biosolids-derived biochar composition, maize growth and nutrition. *Soil and Tillage Research* **165**(Supplement C), 59–65. doi:10.1016/j.still.2016.07.009
- Good J, Ventress L, Knoef H, Zielke U, Hansen PL, Kamp WVD, Wild PD, Coda B, Paasen SV, Kiel J, Sjöström K, Liliedahl T, Unger C, Neeft J, Suomalainen M, Simell P (2005) Sampling and analysis of tar and particles in biomass producer gases, Technical Report prepared under CEN BT/TF 143 “Organic contaminants (“tar”) in biomass producer gases”. Available at <http://www.eeci.net/results/pdf/Technical-Report-version-3-8-final.pdf> [verified May 2018]
- Hannl TK, Haggström G, Hedayati A, Skoglund N, Kuba M, Öhman M (2022) Ash transformation during single-pellet gasification of sewage sludge and mixtures with agricultural residues with a focus on phosphorus. *Fuel Processing Technology* **227**, 107102. doi:10.1016/j.fuproc.2021.107102
- Hedayati A, Lindgren R, Skoglund N, Boman C, Kienzl N, Öhman M (2021) Ash Transformation during Single-Pellet Combustion of Agricultural Biomass with a Focus on Potassium and Phosphorus. *Energy & Fuels* **35**(2), 1449–1464. doi:10.1021/acs.energyfuels.0c03324
- Herzel H, Krüger O, Hermann L, Adam C (2016) Sewage sludge ash — A promising secondary phosphorus source for fertilizer production. *Science of the Total Environment* **542**(Pt B), 1136–1143. doi:10.1016/j.scitotenv.2015.08.059
- Hla SS, Roberts D (2015) Characterisation of chemical composition and energy content of green waste and municipal solid waste from Greater Brisbane, Australia. *Waste Management* **41**, 12–19. doi:10.1016/j.wasman.2015.03.039
- Hla SS, Lopes R, Roberts D (2016) The CO<sub>2</sub> gasification reactivity of chars produced from Australian municipal solid waste. *Fuel* **185**, 847–854. doi:10.1016/j.fuel.2016.08.039
- Hla SS, Ilyushechkin A, Ord L, Roberts D (2020) Database of chemical properties of Australian biomass and waste, v13, CSIRO Data Collection. Available at <https://sc-63-cdc.it.csiro.au/content/19/> [verified December 2020]
- Hodge EM (2009) The coal char-CO<sub>2</sub> reaction at high temperature and high pressure. PhD thesis, School of Chemical Engineering and Industrial Chemistry, University of New South Wales, Sydney, Australia.
- Hwang IH, Ouchi Y, Matsuto T (2007) Characteristics of leachate from pyrolysis residue of sewage sludge. *Chemosphere* **68**(10), 1913–1919. doi:10.1016/j.chemosphere.2007.02.060
- Inguanzo M, Menéndez JA, Fuente E, Pis JJ (2001) Reactivity of pyrolyzed sewage sludge in air and CO<sub>2</sub>. *Journal of Analytical and*

- Applied Pyrolysis* **58–59**(Supplement C), 943–954. doi:10.1016/S0165-2370(00)00143-1
- ISO (2015) ISO 18134-3:2015 Solid biofuels — Determination of moisture content — Oven dry method — Part 3: Moisture in general analysis sample, <https://www.iso.org/standard/61637.html/> [verified on 9 December 2022]
- Jaramillo-Arango A, Fonts I, Chejne F, Arauzo J (2016) Product compositions from sewage sludge pyrolysis in a fluidized bed and correlations with temperature. *Journal of Analytical and Applied Pyrolysis* **121**, 287–296. doi:10.1016/j.jaap.2016.08.008
- Jayaraman K, Gökalp I (2015) Pyrolysis, combustion and gasification characteristics of miscanthus and sewage sludge. *Energy Conversion and Management* **89**(Supplement C), 83–91. doi:10.1016/j.enconman.2014.09.058
- Jensen PA, Frandsen FJ, Dam-Johansen K, Sander B (2000) Experimental Investigation of the Transformation and Release to Gas Phase of Potassium and Chlorine during Straw Pyrolysis. *Energy & Fuels* **14**(6), 1280–1285. doi:10.1021/ef000104v
- Jin J, Li Y, Zhang J, Wu S, Cao Y, Liang P, Zhang J, Wong MH, Wang M, Shan S, Christie P (2016) Influence of pyrolysis temperature on properties and environmental safety of heavy metals in biochars derived from municipal sewage sludge. *Journal of Hazardous Materials* **320**(Supplement C), 417–426. doi:10.1016/j.jhazmat.2016.08.050
- Kirkels AF, Verbong GPJ (2011) Biomass gasification: Still promising? A 30-year global overview. *Renewable and Sustainable Energy Reviews* **15**(1), 471–481. doi:10.1016/j.rser.2010.09.046
- Li QH, Zhang YG, Meng AH, Li L, Li GX (2013) Study on ash fusion temperature using original and simulated biomass ashes. *Fuel Processing Technology* **107**, 107–112. doi:10.1016/j.fuproc.2012.08.012
- Li M, Tang Y, Lu XY, Zhang Z, Cao Y (2018) Phosphorus speciation in sewage sludge and the sludge-derived biochar by a combination of experimental methods and theoretical simulation. *Water Research* **140**, 90–99. doi:10.1016/j.watres.2018.04.039
- Liu H, Wang Y, Hu H, Fu B, Yao H, Wendt JOL (2020) Enrichment mechanism of arsenic in fine ash deposits during co-combustion of rice husk and coal. *Fuel* **281**, 118712. doi:10.1016/j.fuel.2020.118712
- Lu T, Yuan H, Wang Y, Huang H, Chen Y (2015) Characteristic of heavy metals in biochar derived from sewage sludge. *Journal of Material Cycles and Waste Management* **18**(4), 725–733. doi:10.1007/s10163-015-0366-y
- Lundin M, Olofsson M, Pettersson GJ, Zetterlund H (2004) Environmental and economic assessment of sewage sludge handling options. *Resources, Conservation and Recycling* **41**(4), 255–278. doi:10.1016/j.resconrec.2003.10.006
- Midilli A, Dogru M, Howarth CR, Ling MJ, Ayhan T (2001) Combustible gas production from sewage sludge with a downdraft gasifier. *Energy Conversion and Management* **42**(2), 157–172. doi:10.1016/S0196-8904(00)00053-4
- Moon J, Mun T-Y, Yang W, Lee U, Hwang J, Jang E, Choi C (2015) Effects of hydrothermal treatment of sewage sludge on pyrolysis and steam gasification. *Energy Conversion and Management* **103**(Supplement C), 401–407. doi:10.1016/j.enconman.2015.06.058
- Nidheesh PV, Gopinath A, Ranjith N, Praveen Akre A, Sreedharan V, Suresh Kumar M (2021) Potential role of biochar in advanced oxidation processes: A sustainable approach. *Chemical Engineering Journal* **405**, 126582. doi:10.1016/j.cej.2020.126582
- Nilsson S, Gómez-Barea A, Cano DF (2012) Gasification reactivity of char from dried sewage sludge in a fluidized bed. *Fuel* **92**(1), 346–353. doi:10.1016/j.fuel.2011.07.031
- Nilsson S, Gómez-Barea A, Ollero P (2013) Gasification of char from dried sewage sludge in fluidized bed: Reaction rate in mixtures of CO<sub>2</sub> and H<sub>2</sub>O. *Fuel* **105**(Supplement C), 764–768. doi:10.1016/j.fuel.2012.09.008
- Nowicki L, Anteck A, Bedyk T, Stolarek P, Ledakowicz S (2011) The kinetics of gasification of char derived from sewage sludge. *Journal of Thermal Analysis and Calorimetry* **104**(2), 693–700. doi:10.1007/s10973-010-1032-1
- Park HJ, Heo HS, Park Y-K, Yim J-H, Jeon J-K, Park J, Ryu C, Kim S-S (2010) Clean bio-oil production from fast pyrolysis of sewage sludge: Effects of reaction conditions and metal oxide catalysts. *Bioresource Technology* **101**(1, Supplement), S83–S85. doi:10.1016/j.biortech.2009.06.103
- Quispe I, Navia R, Kahhat R (2017) Energy potential from rice husk through direct combustion and fast pyrolysis: A review. *Waste Management* **59**, 200–210. doi:10.1016/j.wasman.2016.10.001
- Raheem A, Sikarwar VS, He J, Dastyar W, Dionysiou DD, Wang W, Zhao M (2018) Opportunities and challenges in sustainable treatment and resource reuse of sewage sludge: A review. *Chemical Engineering Journal* **337**, 616–641. doi:10.1016/j.cej.2017.12.149
- Roberts DG, Harris DJ (2000) Char Gasification with O<sub>2</sub>, CO<sub>2</sub> and H<sub>2</sub>O: Effects of Pressure on Intrinsic Reaction Kinetics. *Energy & Fuels* **14**(2), 483–489. doi:10.1021/ef9901894
- Roy MM, Dutta A, Corscadden K, Havad P, Dickie L (2011) Review of biosolids management options and co-incineration of a biosolid-derived fuel. *Waste Management* **31**(11), 2228–2235. doi:10.1016/j.wasman.2011.06.008
- Rulkens WH, Bien JD (2004) Recovery of energy from sludge – Comparison of the various options. *Water Science and Technology* **50**, 213–221. doi:10.2166/wst.2004.0574
- Sattar A, Leeke GA, Hornung A, Wood J (2014) Steam gasification of rapeseed, wood, sewage sludge and miscanthus biochars for the production of a hydrogen-rich syngas. *Biomass and Bioenergy* **69**(Supplement C), 276–286. doi:10.1016/j.biombioe.2014.07.025
- Saveyn H, Ferrasse JH, Hernandez AB, Rose J, Meerem Pvd, Roche N (2011) The Distribution of Heavy Metals Following Sewage Sludge Gasification. *Journal of Residuals Science and Technology* **8**(2), 61–66.
- Saw W, McKinnon H, Gilmour I, Pang S (2012) Production of hydrogen-rich syngas from steam gasification of blend of biosolids and wood using a dual fluidised bed gasifier. *Fuel* **93**(Supplement C), 473–478. doi:10.1016/j.fuel.2011.08.047
- Scott SA, Davidson JF, Dennis JS, Fennell PS, Hayhurst AN (2005) The rate of gasification by CO<sub>2</sub> of chars from waste. *Proceedings of the Combustion Institute* **30**(2), 2151–2159. doi:10.1016/j.proci.2004.08.061
- Seredych M, Bandosz TJ (2007) Sewage sludge as a single precursor for development of composite adsorbents/catalysts. *Chemical Engineering Journal* **128**(1), 59–67. doi:10.1016/j.cej.2006.06.025
- Shao J, Yan R, Chen H, Wang B, Lee DH, Liang DT (2008) Pyrolysis Characteristics and Kinetics of Sewage Sludge by Thermogravimetry Fourier Transform Infrared Analysis. *Energy & Fuels* **22**(1), 38–45. doi:10.1021/ef700287p
- Shao Y, Tan H, Shen D, Zhou Y, Jin Z, Zhou D, Lu W, Long Y (2020) Synthesis of improved hydrochar by microwave hydrothermal carbonization of green waste. *Fuel* **266**, 117146. doi:10.1016/j.fuel.2020.117146
- Singh RP, Agrawal M (2008) Potential benefits and risks of land application of sewage sludge. *Waste Management* **28**(2), 347–358. doi:10.1016/j.wasman.2006.12.010
- Skoglund N, Båfver L, Fahlström J, Holmén E, Renström C (2016) Fuel design in co-combustion of demolition wood chips and municipal sewage sludge. *Fuel Processing Technology* **141**, 196–201. doi:10.1016/j.fuproc.2015.08.037
- Song W, Guo M (2012) Quality variations of poultry litter biochar generated at different pyrolysis temperatures. *Journal of Analytical and Applied Pyrolysis* **94**, 138–145. doi:10.1016/j.jaap.2011.11.018
- Spanos T, Ene A, Styliani Patronidou C, Xatzixristou C (2016) Temporal variability of sewage sludge heavy metal content from Greek wastewater treatment plants. *Ecological Chemistry and Engineering S* **23**(2), 271–283. doi:10.1515/eces-2016-0019
- Stylianou M, Christou A, Dalias P, Polycarpou P, Michael C, Agapiou A, Papanastasiou P, Fatta-Kassinos D (2020) Physicochemical and structural characterization of biochar derived from the pyrolysis of biosolids, cattle manure and spent coffee grounds. *Journal of the Energy Institute* **93**(5), 2063–2073. doi:10.1016/j.joei.2020.05.002
- Syed-Hassan SSA, Wang Y, Hu S, Su S, Xiang J (2017) Thermochemical processing of sewage sludge to energy and fuel: Fundamentals, challenges and considerations. *Renewable and Sustainable Energy Reviews* **80**, 888–913. doi:10.1016/j.rser.2017.05.262
- Thy P, Jenkins B, Grundvig S, Shiraki R, Leshar C (2006) High temperature elemental losses and mineralogical changes in common biomass ashes. *Fuel* **85**(5–6), 783–795. doi:10.1016/j.fuel.2005.08.020
- Tippayawong N, Chaichana C, Promwungkwa A, Rerkkriangkrai P (2013) Investigation of a Small Biomass Gasifier–engine System

- Operation and Its Application to Water Pumping in Rural Thailand. *Energy Sources, Part A: Recovery, Utilization, and Environmental Effects* **35**(5), 476–486. doi:10.1080/15567036.2010.511433
- Tyagi VK, Lo S-L (2013) Sludge: A waste or renewable source for energy and resources recovery? *Renewable and Sustainable Energy Reviews* **25**(Supplement C), 708–728. doi:10.1016/j.rser.2013.05.029
- Tytła M, Widziewicz K, Zielewicz E (2016) Heavy metals and its chemical speciation in sewage sludge at different stages of processing. *Environmental Technology* **37**(7), 899–908. doi:10.1080/09593330.2015.1090482
- Vassilev SV, Baxter D, Andersen LK, Vassileva CG, Morgan TJ (2012) An overview of the organic and inorganic phase composition of biomass. *Fuel* **94**, 1–33. doi:10.1016/j.fuel.2011.09.030
- Werle S (2015) Gasification of a Dried Sewage Sludge in a Laboratory Scale Fixed Bed Reactor. *Energy Procedia* **66**(Supplement C), 253–256. doi:10.1016/j.egypro.2015.02.046
- Werle S, Dudziak M (2014) Gaseous fuels production from dried sewage sludge via air gasification. *Waste Management & Research* **32**(7), 601–607. doi:10.1177/0734242X14536460
- Xu M, Li D, Yan Y, Guo T, Pang H, Xue H (2017) Porous high specific surface area-activated carbon with co-doping N, S and P for high-performance supercapacitors. *RSC Advances* **7**(69), 43780–43788. doi:10.1039/C7RA07945A
- Zheng S, Yang Y, Li X, Liu H, Yan W, Sui R, Lu Q (2020) Temperature and emissivity measurements from combustion of pine wood, rice husk and fir wood using flame emission spectrum. *Fuel Processing Technology* **204**, 106423. doi:10.1016/j.fuproc.2020.106423

**Data availability.** The data that support this study are available in the article.

**Conflicts of interest.** The authors declare no conflicts of interest.

**Declaration of funding.** This research did not receive any specific grant from funding agencies in the public, commercial, or not-for-profit sectors.

**Acknowledgements.** The authors are grateful to Queensland Urban Utilities for their assistance and arrangement for collection of biosolid samples. We acknowledge Mr Mark Kochanek for his guidance and assistance with the operation of experimental equipment used in this study.

**Author affiliation**

<sup>A</sup>CSIRO Energy, PO Box 883, Kenmore 4069, Australia.